Influence of Porosity on Fracture Toughness and Fracture Behavior of Antibiotic-Loaded PMMA Bone Cement

Sunjung Kim
Mechanical Engineering,
University of Wisconsin – Madison,
Madison, WI 60085

Caroline Baril
Mechanical and Materials Engineering,
Queen's University,
Kingston, ON K7L 3N6, Canada

Shiva Rudraraju
Mechanical Engineering,
University of Wisconsin – Madison,
Madison, WI 60085

Heidi-Lynn Ploeg[1]
Mechanical Engineering,
University of Wisconsin – Madison,
Madison, WI 60085;
Department of Mechanical and
Materials Engineering,
Queen's University,
McLaughlin Hall,
130 Stuart St.,
Room 303B,
Kingston, ON K7L 3N6, Canada
e-mail: heidi.ploeg@queensu.ca

Aseptic loosening is the most common reason for the long-term revision of cemented arthroplasties with fracture of the cement being a postulated cause or contributing factor. In our previous studies we showed that adding an antibiotic to a polymethylmethacrylate (PMMA) bone cement led to detrimental effects on various mechanical properties of the cement such as bending strength, compressive strength and fracture toughness (K_{IC}). This finding implied that the mechanical failure of antibiotic-loaded PMMA bone cement was influenced by its pore volume fraction. Up to now this aspect has not been studied. Hence the purposes of this study were to determine (1) the influence of antibiotic (telavancin) loading on the K_{IC} of a widely used PMMA bone cement brand (Palacos®R) and (2) the influence of pore size and pore distribution on the fracture behavior of the K_{IC} specimens. For (2) both experimental and numerical methods (extended finite element method [XFEM]) were used allowing a comparison between the two sets of results. We found that: (1) K_{IC} decreased with increased porosity with the drop (relative to the value for the control cement) being significant when the telavancin loading was 4.8 wt/wt% (2 g of telavancin added to 40 g of control cement powder); (2) there was a critical pore size above which there was a significant decrease in K_{IC} and is 1 mm; (3) crack propagation was strongly influenced by pore size and pore locations (pore–pore interactions); and, (4) there was good agreement between the experimental and XFEM results. The implications of these findings for the use of a telavancin-loaded PMMA bone cement in cemented total joint arthroplasties are commented upon. [DOI: 10.1115/1.4051848]

Keywords: antibiotic-loaded PMMA bone cement, fracture toughness, pore size and distribution, extended finite element analysis

1 Introduction

Polymethylmethacrylate (PMMA) bone cement is a well-known biomaterial used for anchoring cemented arthroplasties [1]. The main role of bone cement is to transfer load from the implant to the bone. The survival rate of cemented hip stem fixation is over 88% for the last 15 years [2]. Despite the high success rate, cement use has been controversial. One of the major drawbacks is aseptic loosening, the most common reason (57.5%) for mechanical failure [3–5]. The cement is a material discontinuity between the implant and the bone, making the cement prone to fracture [6]. This failure mechanism is considered the primary mechanism of aseptic loosening in cemented arthroplasty [6,7].

The clinical use of bone cement has been investigated by many researchers. Numerous laboratory studies have focused on antibiotic-loaded PMMA bone cement (ALBCs) to reduce the risk of infection after arthroplasty surgery. Some authors have demonstrated, however, that cement either with or without antibiotics has degraded mechanical strength [8,9]. There is concern that adding antibiotics to bone cement weakens the cement, resulting in early failure of the implant [10–12]. As reported by Sanz-Ruiz et al., different antibiotics have different effects on the mechanical properties of cement [13]. On the other hand, Van de-Belt et al. reported that the type of bone cement used determined the surface roughness, porosity, antibiotic release, and wettability of antibiotic-loaded bone cements, which might affect the cement strength [14].

Some studies have shown that pores can act as crack initiation and propagation sites [15,16]. These findings prompted the development of mixing techniques to reduce porosity, such as mixing in a vacuum and centrifuging. These mixing methods successfully showed a substantial reduction in the porosity and increased the cement strength [17–19]. Seyyed Hosseinzadeh noted that when the pores reached a critical size, pores acted as sites of stress concentration, leading to cement weakening. Pores below this critical size acted as crack arrestors; therefore, the authors emphasized eliminating pores greater than the critical size [20]. Pore density and distribution, apart from the overall bulk porosity, are other important factors. Hoey and Taylor [21] demonstrated that pore clustering was detrimental to fatigue properties of bone cement. Jeffers et al. [22] in their simulations of cement porosity using finite element analysis (FEA) found that cement porosity may facilitate fatigue cracking of the cement mantle. Despite numerous studies, performed to identify the effect of porosity on bone cement, a thorough comparative study of experimental and numerical predictions to investigate the K_{IC} and crack behavior of ALBC has not been carried out. This paper describes such a study using fracture experiments and the numerical extended finite element method (XFEM) [23–25] to investigate crack evolution in an ALBC.

The objectives of this study were to: (1) use an experimental method to determine the influence of the amount of antibiotic added to the powder of a PMMA bone cement on its K_{IC}; (2) use an experimental method to determine the influence of pore size and distribution in a K_{IC} specimen on its fracture behavior; (3) use a numerical method (XFEM) to determine the influence of pore size and distribution in a K_{IC} specimen on its fracture behavior; and, (4) compare the results obtained from objectives (2) and (3).

---

[1] Corresponding author.

Manuscript received March 21, 2021; final manuscript received July 8, 2021; published online September 1, 2021. Assoc. Editor: Joseph Wallace.

2 Materials and Methods

2.1 Materials. Six different experimental groups were prepared based on different amounts of added antibiotic (telavancin; Theravance Biopharma US, Inc., CA). The bone cement (Palacos® R) with no antibiotic served as a control group and five telavancin-loaded bone cement groups were prepared with antibiotic masses at 0.3, 0.6, 1.2, 2.4, and 4.8 wt/wt %, respectively, with seven specimens per group. For each of the cement formulations, 40 g of cement powder and telavancin were mixed by hand for 1 min in a syringe. The blended powder (control cement powder and added telavancin) was vacuum mixed with the control cement liquid (−5 kPa) [26], and the resulting mixture was poured into an aluminum mold, whose configuration and dimensions were as specified in ASTM-D5045 for plane strain fracture toughness testing. The fracture toughness specimens were 44 mm long, 5 mm wide, and 10 mm high, with a 5 mm pre-existing crack. Cracks were created using a diamond wafering blade (Buehler® Iso-MetTM, Lake Bluff, IL). The crack length was measured from images using IMAGEJ (National Institutes of Health and the Laboratory for Optical and Computational Instrumentation, Madison, WI). Each specimen was cured in a 1×phosphate-buffered saline (PBS) for 21 days at 21 °C before testing [27]. After the conditioning in PBS, the specimen was taken directly from PBS for testing.

2.2 Mechanical Testing. Single-edge notched bend testing (Fig. 1(*a*)) in air at room temperature was applied to the three-point bending specimens with a displacement rate control mode of 10 mm/min until fracture. The applied bending load was recorded synchronously with crosshead displacement. K_{IC} (MPa$\sqrt{m}$) was calculated according to ASTM-E399-08. For single-edge notched bending test, the bending stress (σ_b) and mode I K_{Ic} were found from Eqs. (1) [28] and Eq. (2) based on ASTM-E399-08, respectively,

$$\sigma_b = \frac{3PS}{2b(h-a_c)^2} \tag{1}$$

$$K_{IC} = \frac{3PS}{2bh^{3/2}} f(x) \tag{2}$$

where P is the load, a_c is the length of the notch, b and h are, respectively, the width and height of the specimen, and S (32 mm) is the span between the two lower supporting points. The lengths are in mm, and the force is in N. f is a function of a_c/h, given by Eq. (3) (ASTM-E399-08)

$$f\left(\frac{a_c}{h}\right) = 1.93\left(\frac{a_c}{h}\right)^{\frac{1}{2}} - 3.07\left(\frac{a_c}{h}\right)^{\frac{3}{2}} + 14.53\left(\frac{a_c}{h}\right)^{\frac{5}{2}} - 25.11\left(\frac{a_c}{h}\right)^{\frac{7}{2}} + 25.80\left(\frac{a_c}{h}\right)^{\frac{9}{2}} \tag{3}$$

2.3 Extended Finite Element Method. Extended finite element method is a popular advancement of the classical finite element method (FEM) that is used to model discontinuities, especially fracture in materials. In XFEM, additional degrees-of-freedom are added at the finite element nodes in the neighborhood of the crack path. These additional degrees-of-freedom are used to represent the displacement discontinuity induced by the presence of a crack, without much alteration to the underlying FEM mesh. The displacement interpolation of the XFEM is given by Eq. (4)

$$u(x) = \sum_{I=1}^{N} N_I(x)\left[u_I + H(x)a_I + \sum_{a}^{4} F_a(x){b_I}^a\right] \tag{4}$$

where $u(x)$ is displacement, $N_I(x)$ is the conventional finite element shape function, $H(x)$ is the discontinuous shape function, a_I is the added set of degrees-of-freedom to the standard finite element model, F_a is the crack tip enrichment function, and ${b_I}^a$ is the degree-of-freedom of the enrichment node.

Extended finite element method available in the commercial finite element software ABAQUS v.6.11 (Dassault Systèmes Simulia Corp., Johnston, RI) was implemented for the simulation results in this work. We modeled 2D geometries and assumed a plane strain material model for the bone cement. The modulus of elasticity, $E = 2080$ MPa, obtained from the four-point bending test was used for the material properties of PMMA bone cement. In order to determine the crack initiation, the maximum principal stress criterion was considered. Under this criterion, Mode-I crack initiation and growth occur when the principal stress is equal to or greater than the yield strength of material. This is a good criterion for brittle materials like bone cement, where the yield limit is close to the ultimate strength of the material. A yield strength, $\sigma_y = 54$ MPa, was obtained from uniaxial compression tests and was used as an input for the Maximum Principal Stress criterion [29,30]. Both mechanical properties (E and σ_y) were experimentally obtained from the control group (no pores) as described in detail in our previous study [26]. A Poisson's ratio of 0.4 [31] was considered.

Figure 1(*b*) shows a 2D XFEM model of the bending fracture test setup for a bone cement specimen with randomly distributed pores of the same size. The mesh consisted of 2000–3000 four-node bilinear plane strain quadrilateral and reduced integration elements. A mesh convergence study found maximum von Mises stress converged for this element size. The top and bottom supports were modeled as rigid surfaces. The bottom supports were fixed in all directions, and displacement of the top support was applied by controlling the displacement of the reference point. A friction coefficient of zero between the steel roller support and the PMMA bone cement specimen was assumed. The constitutive response representing crack initiation and evolution was modeled as a cohesive zone with damage evolution (Fig. 2), and the

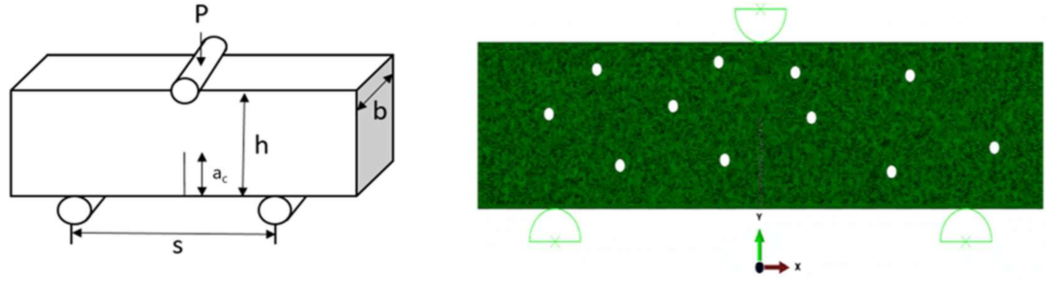

(*a*) (*b*)

Fig. 1 (*a*) Schematic of the single-edge notched bending test. *P* denotes the bending force, a_c is the length of the notch, *b* and *h* are, respectively, the width and height of the specimen, and *s* is the span between the two lower supporting points. (*b*) two-dimensional (2D) mesh for XFEM of a notched bone cement specimen with pores under the single-edge notched bending test.

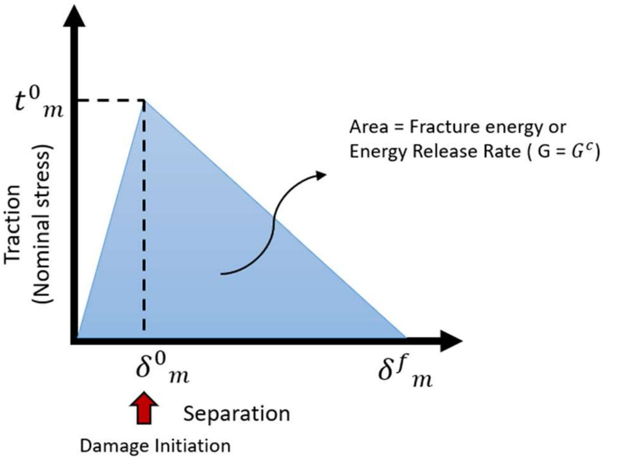

Fig. 2 Damage evolution represented by a cohesive traction separation law. The triangular cohesive law contains two critical parameters: the cohesive strength, t^0_m (the maximum traction the interface can endure), or the separation length, δ^0_m, and the cohesive energy, which is the area of the triangle. The critical strain energy rate, G_c, corresponds to the area under the traction-separation curve.

maximum principal stress criterion was selected as the damage criterion for the traction separation law. The maximum principal stress criterion identifies the point of crack initiation and also provides a direction criterion (perpendicular to the maximum principal stress direction) for crack propagation. The fracture energy release rate (G) of 3712 J/m^2 was calculated from our previous experimental results for K_{IC} and elastic modulus ($K_{IC} = 2.70\,\mathrm{MPa}\sqrt{\mathrm{m}}$ and $E = 2080\,\mathrm{MPa}$) obtained for the control group to characterize crack propagation [26].

2.4 Pore Size and Location for Modeling. The mechanism of crack growth and the toughening of bone cement are complex in part due to its porous microstructure. The pore-related parameters that affect crack growth and propagation can be divided into independent parameters such as pore shape and dependent parameters such as pore-pore and pore-crack interactions. The interactions of the dependent parameters are affected by pore size and location. In this study, therefore, three different conditions were tested with ten models per condition:

(I) Pore locations were fixed, and each pore diameter was increased from 0.2 to 1.0 mm in 0.2 mm increments. Three different fixed pore locations were tested.
(II) Pore locations were randomly distributed, and each pore diameter was fixed at 0.2 mm, 0.6 mm, and 1.0 mm.
(III) Pore locations were randomly distributed, and a normal distribution of each diameter (0.2 ± 0.07, 0.6 ± 0.2, 1.0 ± 0.18 mm) was assigned together in a single model.

These three conditions were created ten times each according to the pore locations and size distributions described above. The number of pores were determined such that the resulting pore volume fraction matched the micro-CT and water uptake porosity measurements.

2.5 Porosity Measurement by Microcomputed Tomography (CT) Scanning. The porosities of the specimens were determined using a microcomputed tomography (CT) system (Micro-XCT400, Xradia, Oberkochen, Germany), with an acquisition protocol that comprised: X-ray tube setting of 80 kV, 9 W, and 100 μA, exposure time of 0.5 s, and 100 frame averaging. Four specimens were mounted on a rotary stage and scanned in their entirety, being rotated −92 deg to 90 deg in equiangular steps. The associated per-scan times took approximately 1 h. The stack of 2D images consisted of 400 slices, 40 mm fields of view, 38 μm pixel size, and 40 μm isotropic voxel size. The images were imported into Mimics Innovation Suite 20.0 (Materialise NV, Leuven, Belgium) to obtain three-dimensional (3D) models of the specimens. The images were segmented by an operator-selected threshold of gray scale values to separate the voxels representing bone cement. The 3D models were analyzed to obtain porosity by quantifying the bulk and pore volumes in the specimen. Micro-CT porosity measurements were validated against water uptake porosity measurements. Porosity was quantified using Archimedes' principle with bulk volume measured with digital vernier calipers, specimen dry mass measured in air, and wet mass measured after 24 h submersed in de-ionized water.

2.6 Scanning Electron Microscopy for Pore Size Measurement. The external and fracture surfaces of the K_{IC} specimens following the test were examined using a scanning electron microscope (SEM; Zeiss-LEO, Oberkochen, Germany). A thin layer of platinum was deposited on the specimen surfaces for 35 s with 45 mA. Images were obtained at 200x magnification using an acceleration voltage of 3 kV. The pore size and numbers were quantified.

2.7 Statistical Analysis of Mechanical Test Data. The mechanical testing results were statistically assessed using Minitab 18 (Minitab Inc., State College, PA). The Kolmogrov–Smirnov method was used to test the normality assumption. Kruskal–Wallis and posthoc Mann–Whitney U tests were conducted for nonparametric comparison between the control and the telavancin-added groups. The results are presented as the mean-standard error of the mean. A p-value of less than 0.05 was considered statistically significant.

3 Results

3.1 Fracture Toughness Test Results. The K_{IC} of each of the telavancin-loaded cements was lower than that of the control cement. ($2.70 \pm 0.22\,\mathrm{MPa}\sqrt{\mathrm{m}}$), but the decrease was significant only for the cement formulation with 4.8 wt/wt % telavancin ($2.10 \pm 0.15\,\mathrm{MPa}\sqrt{\mathrm{m}}$) (Fig. 3).

The experimental load–displacement curves for the control group specimens (Fig. 4) overlapped most closely with each other, while the groups with added telavancin showed more variance in stiffness between specimens. In addition, the peak force for the 4.8 wt/wt % of added telavancin group (137 ± 13.6 N) showed a

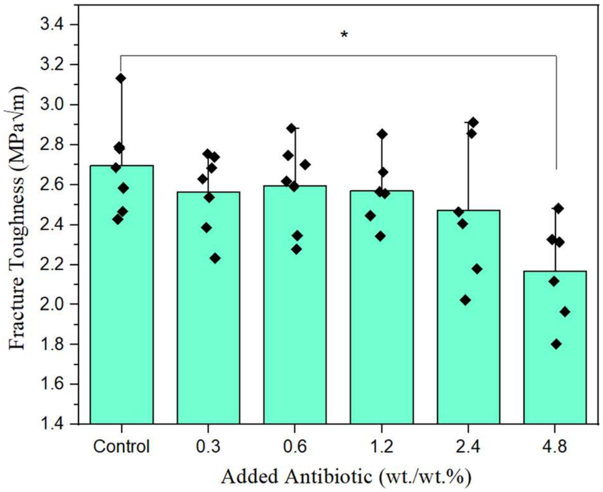

Fig. 3 K_{IC} values are shown as the mean and standard error of the mean for the specimen in each group. The asterisk represents a significant ($p < 0.05$) difference from control group.

Table 1 Pore volume fraction of the control group and five groups with different amounts of added antibiotic. The pore volume fractions, measured from micro-CT data from specimen, are represented as the mean±SEM. The asterisk indicates a significant difference from the control group ($p < 0.05$).

	Antibiotic mass ($n = 8$)					
	Control	0.3 wt/wt %	0.6 wt/wt %	1.2 wt/wt %	2.4 wt/wt %	4.8 wt/wt %
Pore volume fraction (%)	4.49 ± 0.32	4.70 ± 0.30	5.59 ± 0.15*	5.09 ± 0.22*	5.92 ± 0.35*	7.09 ± 0.47*

significant decrease when compared to the control group (160 ± 12.3 N).

Scanning electron microscope images (Fig. 5(*b*)) of the bone cement specimen fracture surfaces show “mirror,” “mist”, and “hackle” zones. The mirror zone is formed during the crack growth phase. The mist zone is created by slow crack propagation. Here, however, there was no noticeable difference between the mirror and the mist zones. The hackle zone is created by rapid

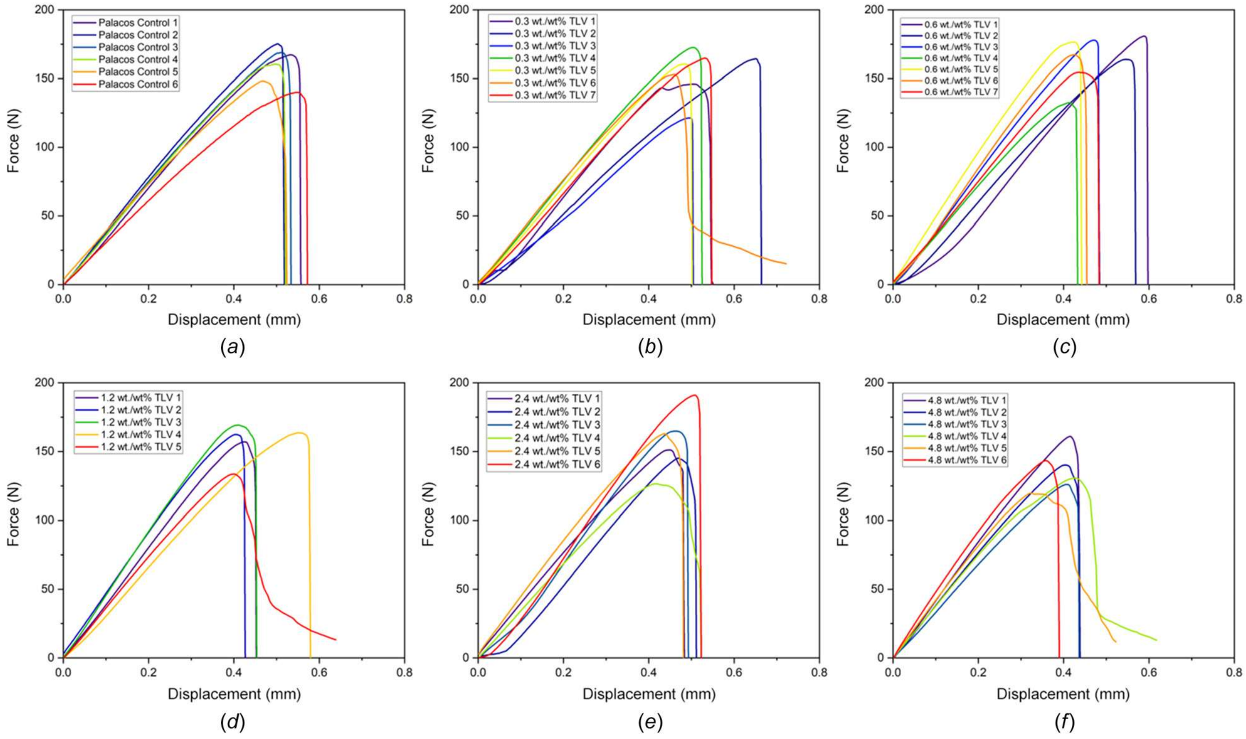

(*a*) (*b*) (*c*)

(*d*) (*e*) (*f*)

Fig. 4 Experimental load–displacement curves for the specimen groups with different amounts of added telavancin

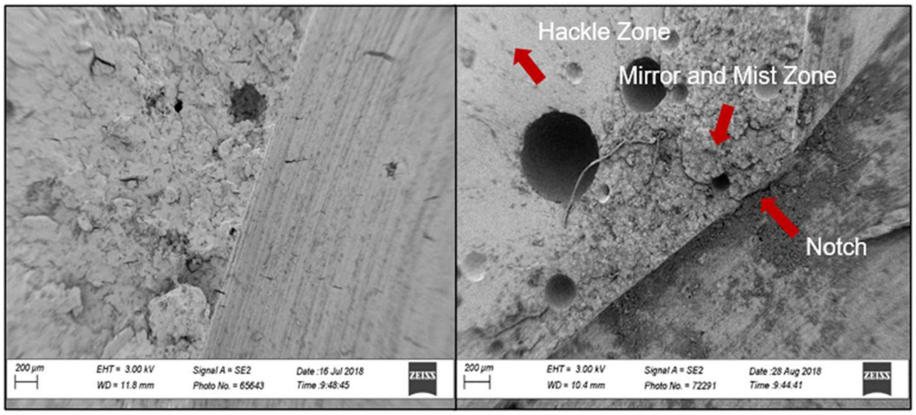

(*a*) (*b*)

Fig. 5 Micrographs of the fracture surface following the test at 200× magnification showing (*a*) the control specimen and (*b*) the cement loaded with 4.8 wt/wt% telavancin containing the mirror, mist and hackle zones of the crack propagation surface

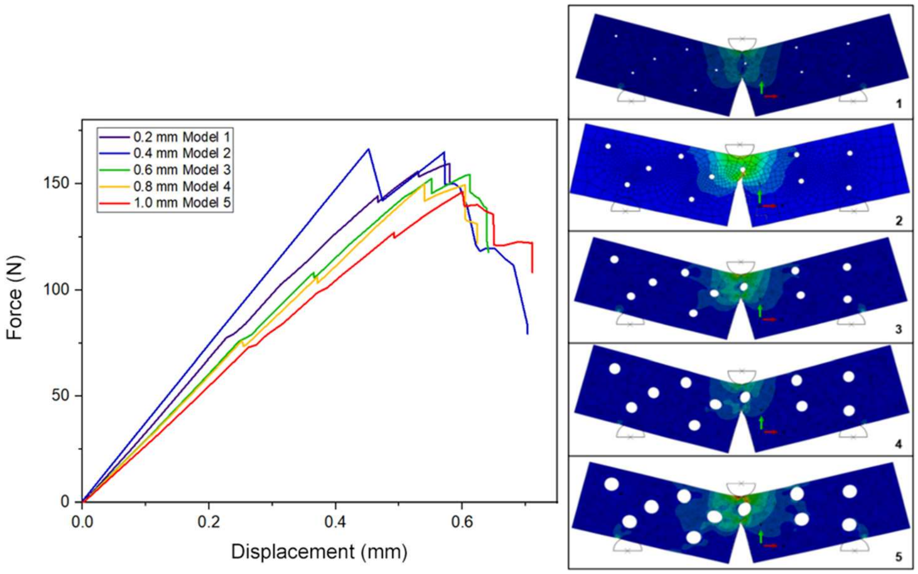

Fig. 6 Numerical load–displacement curves for 0.2, 0.4, 0.6, 0.8, and 1.0 mm pore size with fixed locations corresponding to the pore volume fraction of 0.31, 1.25, 2.82, 5.02, and 7.85%, respectively. The FEA models on the right show corresponding examples of the von Mises stress distributions. The stress range is the same for all plots: 0 MPa (min) to 90 MPa (max).

crack propagation. In the hackle zone, the surface appeared much smoother and flatter than in the other two zones.

3.2 Pore Volume Fraction Measurement Results. Macropores were observed in SEM images of the fracture surface for the 4.8 wt/wt % antibiotic group, while micropores were found in the control group (Fig. 5). The pore volume fraction of the telavancin-loaded cement was significantly greater than in the control cement, except for the 0.3 wt/wt % telavancin group. The increased pore volume fractions starting at 0.6 wt/wt % loading resulted from a combination of many micropores and a few macropores, both of which were rarely seen in the control and 0.3 wt/wt %. The increased pore volume fractions for the 0.6 wt/wt % loading and higher were statistically differ from the control group (Table 1). The pore volume fraction was divided into two groups: small dose (0.3, 0.6 and 1.2 wt/wt %, 4.70 ± 0.30 to 5.09 ± 0.22%) and large-dose (2.4 and 4.8 wt/wt %, 5.92 ± 0.35 to 7.09 ± 0.47%). The small-dose specimens did not significantly different from each other, and neither did the large-dose specimens significantly differ from each other ($p < 0.05$).

3.3 Extended Finite Element Method Simulation Results. The results of the three different simulation cases were compared with the experimental load–displacement data. For case I, all three models produced similar load–displacement patterns. The change in pore size significantly impacted the load–displacement curves (Fig. 6). A reductions in the peak force and stiffness were observed for the increased pore size and pore volume fraction.

The effect of pore location, based on testing five different models containing randomly distributed pores with fixed diameters of 0.2 mm, is shown in Fig. 7(*a*). The influence of pore location on both peak force and stiffness was marginal, but the behavior following crack initiation varied. These trends were also found with fixed pore diameter of 0.6 and 1.0 mm (Fig. 7(*b*)).

Figure 8 shows the results for case III, where the pore locations were randomly distributed and normal distributions for each diameter (0.2 ± 0.07, 0.6 ± 0.2, and 1.0 ± 0.18 mm) were assigned. The load–displacement behavior for the 0.2 mm models closely overlapped with each other up to the peak point, and then slightly differed due to variances in crack propagation patterns. On the other hand, differences in stiffness and peak force were found in the models with larger average pore diameters. The difference between Figs. 7(*b*) and 8(*b*) suggests that pore size affects the load–displacement behavior significantly more than the randomness of the pore location.

3.4 Comparison of Experimental and Simulation Results. The XFEM results showed good agreement with the experimental load–displacement response for the control and 0.3 wt/wt % groups, and varied in stiffness in the other groups (Fig. 9). The 0.6, 1.2, 2.4, and 4.8 wt/wt % specimens exhibited similar peak forces to the experimental values, but with reduced stiffness. The control and 0.3 wt/wt % groups showed the most similar load–displacement response for the 0.6 mm model in Case III and the 0.2 mm model in case II, respectively.

4 Discussion

The effect of antibiotic addition on the K_{IC} of PMMA bone cement was experimentally investigated. The results from the control specimen of Palacos R ($2.70 \pm 0.22\ \mathrm{MPa}\sqrt{m}$) were similar to those of a previous study ($2.69 \pm 0.07\ \mathrm{MPa}\sqrt{m}$) [26]; however, the values were relatively higher than those reported in other studies. Values of 1.70 [32], 1.79 [33], 1.85 $\mathrm{MPa}\sqrt{m}$ [34] for a Palacos R control specimen have been published. The K_{IC} was significantly reduced after adding 4.8 wt/wt % of telavancin to the bone cement. A reduced K_{IC} after adding antibiotic has been illustrated in other studies. Lewis reported that an increase in antibiotic loading from 2.5 to 5.0 wt/wt % led to a significant decrease in the fracture toughness [35]. Similarly, the K_{IC} of gentamicin-loaded Zimmer LVC cement (5.0 wt/wt %) was significantly lower than that of the plain cement [36]. Bishop et al., in studying the effects of vancomycin added to Palacos R, found that the K_{IC} for 4.8 wt/wt % ($2.18 \pm 0.17\ \mathrm{MPa}\sqrt{m}$) was 19% less than in the control ($2.69 \pm 0.07\ \mathrm{MPa}\sqrt{m}$) [26]. Extending these studies, our observations suggest an inverse relationship between the mass of added antibiotic and K_{IC}. This finding is supported by the overall pore volume fraction measurements, which determined significant increases with the mass of added antibiotic. This result demonstrates the relationship between the pore volume fraction and K_{IC} at different doses of added antibiotic.

The influence of PMMA bone cement porosity on its K_{IC} is a controversial issue, with some studies stating that pores are essentially defects and should be removed [19,37], while others posit that pores are required for drug elution, bone ingrowth, and also as a method of blunting cracks [14,38]. Here, pore size was found to be a dominant contributor to K_{IC} reduction. Although a high level of pore volume fraction was observed with 2.4 wt/wt % added antibiotic, the critical force for crack initiation remained unaffected, since the pore sizes were below critical. For the 4.8 wt/wt % group, a lower critical force was required for crack initiation despite a similar level of pore volume fraction to the 2.4 wt./wt % group. Gustafsson et al. demonstrated that the porosity levels were reflected in the load–displacement response, where an increased pore volume fraction rendered lower structural stiffness as well as lowered peak force along with an increased ability to absorb energy before failure [39].

For the cases with distributed pore locations, pores under 1.0 mm had no effect on the K_{IC}; however, pores over 1.0 mm increased pore–pore interactions and the likelihood of failure. Thus, we identify 1.0 mm as a critical size for the pores to begin impacting fracture evolution. The methodology presented here can be extended to other compositions of bone cement and a critical pore size can be estimated. Since crack propagation is driven by crack initiation traction and the energy release rate (G) in the cohesive damage model [39,40], the crack path varies depending on the pore location relative to the crack tip. This is to be expected because the presence of pores significantly alters the stress and the local strain energy distributions, and this affects the crack path dictated by the fracture model.

It is not clear whether porosity is the main factor in failure in the cement mantle in vivo [37,38,41]. However, it is clear that porosity was detrimental to the K_{IC} in the material test specimens with the pore sizes and locations in this study. Similar results have been found by others [19,37]. Porosity has also shown beneficial effects for the clinic. Antibiotic is typically added to the cement for the treatment and prevention of prosthetic joint infection in the surgical area. The elution of antibiotic from cement increases with surface roughness and porosity [14]. In addition, the porosity may

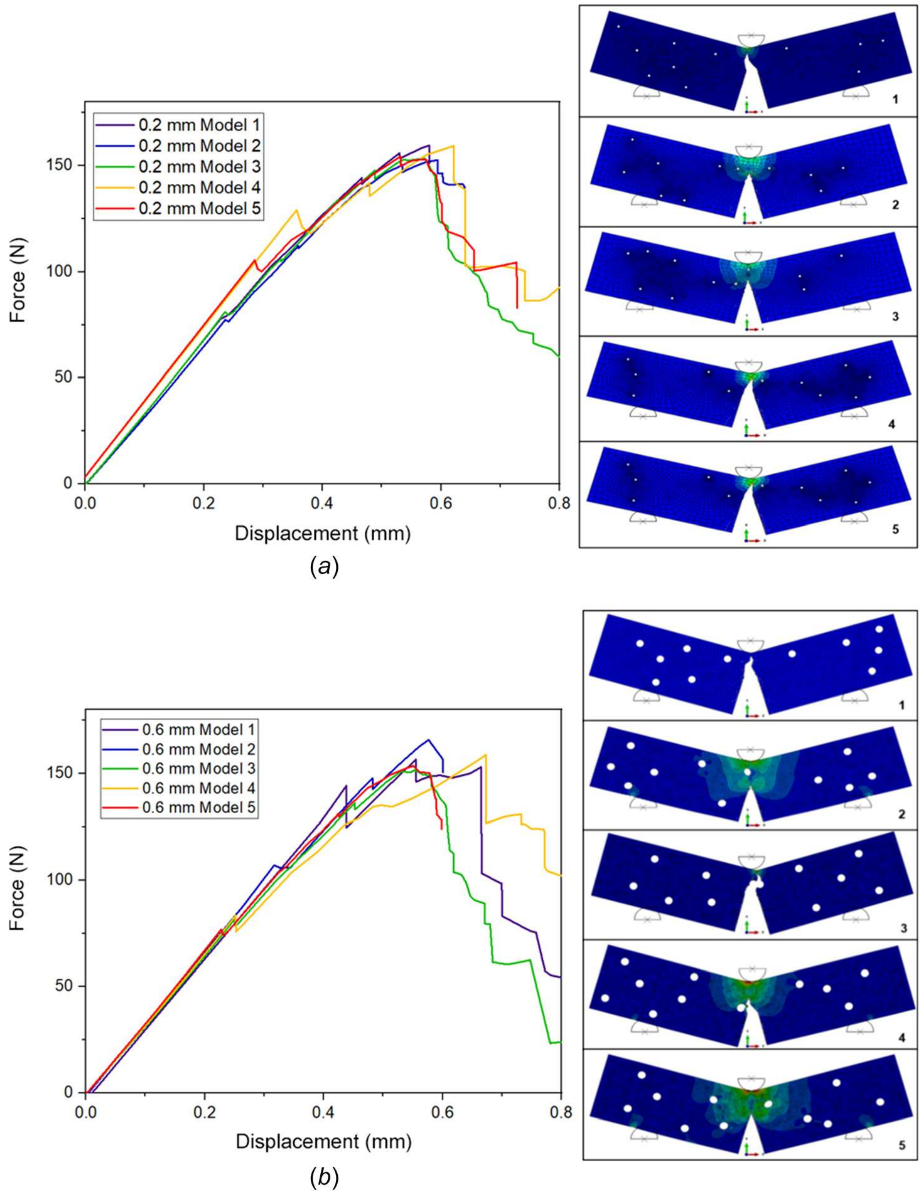

(*a*)

(*b*)

Fig. 7 Numerical load–displacement curves for (*a*) 0.2 mm and (*b*) 0.6 mm pore sizes with random locations. The FEA models on the right show corresponding examples of the von Mises stress distributions. The stress range is the same for all plots: 0 MPa (min) to 90 MPa (max).

increase the cement K_{IC} by dispersing the energy at the crack tip, forming a larger damage zone, and effectively blunting the crack [42]. Therefore, a compromise between the positive and negative effects is essential to finding the best solution. The compromise solution, as suggested by our results, may be an even distribution of micropores for effective antibiotic elution and a reduction of the macropores that decrease the K_{IC}.

The results herein suggest that antibiotic loading at less than 4.8 wt/wt % is appropriate for clinical use to avoid decreased fracture toughness. However, these results need to be taken together with antibiotic elution and efficacy testing. To date, the use of commercially available ALBC products has been cleared by the United States Food and Drug Administration only for use in the second stage of a two-stage joint revision, following elimination of an active infection in the joint, and their antibiotic loading are either 1.2 or 2.4 wt/wt % (equivalent to 0.5 g or 1.0 g added to 40 g of cement powder) [43]. However, it is important to note that the measurements of the bone cement K_{IC} with the aforementioned antibiotic loadings depend on a wide range of parameters, including specimen configuration and size, mixing method, specimen curing method, and aging methods [1].

This study has a number of limitations. First, only one control cement brand was used (Palacos R); more importantly, this brand is classed as "high viscosity" but medium (e.g., Simplex P) and low (e.g., Palacos LV+G) viscosity brands are also used in clinical practice. Second, the resolution of the micro-CT equipment used (38 μm) was too large to measure pores smaller than 40 μm in diameter. These micropores were not included in the FE models and may be the reason for under-prediction of the stiffness. We measured micropores with a water-uptake experiment to validate the micro-CT pore volume fraction. Neither measures of pore volume fraction was significantly different ($p < 0.05$). Third, the XFEM predictions were performed using 2D models; the predictions may be different if 3D models are used [44,45]. However, it

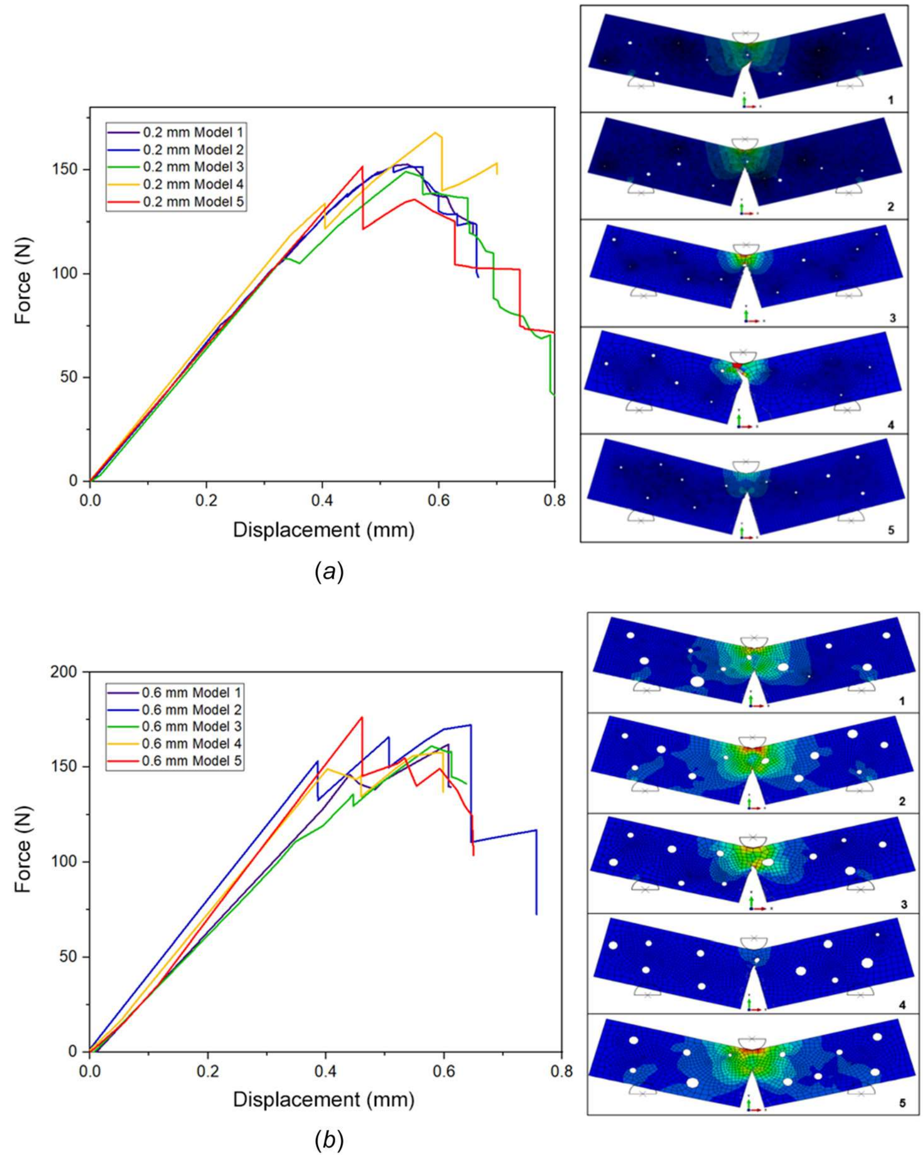

(*a*)

(*b*)

Fig. 8 Numerical load–displacement curves for (*a*) 0.2±0.07 mm and (*b*) 0.6±0.2 mm of average pore size with random locations. There was no significant difference in the results in Fig. 8(*a*) where a pore diameter of 0.2±0.07 mm was randomly assigned. This case corresponded to a level of porosity of less than 5% and below the critical pore size. The FEA models on the right show corresponding examples of the von Mises stress distributions. The stress range is the same for all plots: 0 MPa (min) to 90 MPa (max).

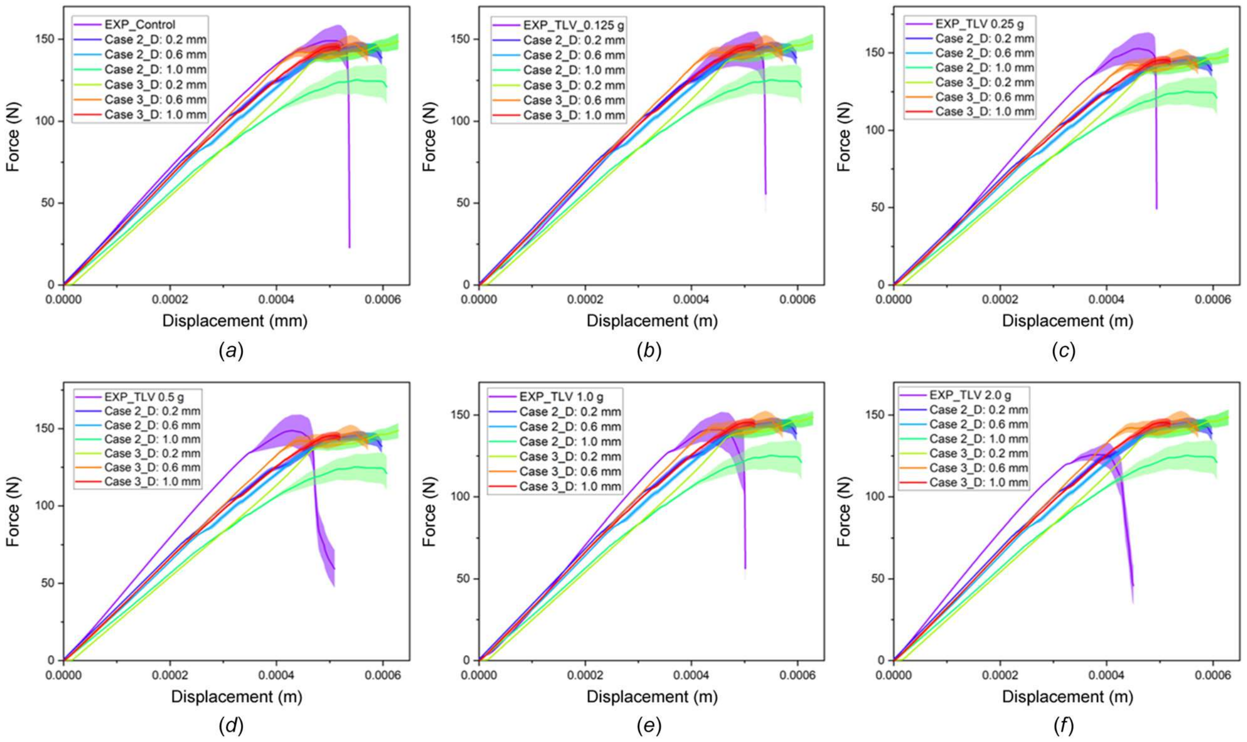

(*a*) (*b*) (*c*)

(*d*) (*e*) (*f*)

Fig. 9 Comparison of load–displacement data from experiments and numerical simulations of fracture in bone cement for (*a*) the control group and groups with different amounts of added antibiotic: (*b*) 0.3 wt/wt %; (*c*) 0.6 wt/wt %; (*d*) 1.2 wt/wt %; (*e*) 2.4 wt/wt %; and (*f*) 4.8 wt/wt %. The load–displacement curves illustrate the mean and the standard error of the mean.

is standard practice in the fracture mechanics community to model 2D equivalents of 3D models, and often the 2D predictions are sufficient [25,46]. This seems to be the case for our model, as the 2D simulation results obtained were similar to the experimental results, and showed an inverse relationship between the porosity and the K_{IC}. The mechanical properties for the XFEM predictions were assumed using data from mechanical tests performed previously by the authors (E and σ_y) and from the literature (Poisson's ratio). Fourth, it is expected that the fracture behavior of telavancin-loaded PMMA bone cement in vivo will be more complex than that displayed in the tests performed in this study; and hence, some deviations in the results for more complex geometries of in vivo specimens may occur. Finally, the loading was applied in a quasi-static condition. In reality, the service loading experienced by an arthroplasty is dynamic with fluctuating forces, and this might produce a discrepancy with the results of this study. Material fatigue testing is significantly more time and resource intensive than fracture toughness testing; however, fracture toughness is generally related to fatigue strength [47]. Therefore, fracture toughness testing can provide insights into material fatigue properties with many variations of specimens (e.g., several amounts of added antibiotic) and produce valuable data for the efficient running of subsequent material fatigue tests for the critical cases.

5 Conclusions

The influence of porosity on the fracture toughness of ALBC has been experimentally determined, and interesting pore size effects were studied using relevant XFEM method-based numerical simulations of crack propagation. The study found:

(1) The K_{IC} of each of the telavancin-loaded cements was lower than that of the control cement ($2.70 \pm 0.22\ \mathrm{MPa}\sqrt{\mathrm{m}}$), but the decrease was significant only for the cement formulation that contained 4.8 wt/wt % telavancin ($2.10 \pm 0.15\ \mathrm{MPa}\sqrt{\mathrm{m}}$).

(2) The pore volume fraction was divided into small (0.0 and 0.3 wt/wt%) and large dose (0.6–4.8 wt/wt%) groups with the mean values being 4.49–4.70% and 5.09–7.09%, respectively.

(3) The numerical simulation indicated the existence of a critical pore size for crack propagation and that the fracture toughness of ALBC was significantly reduced by macro pores, which tended to initiate cracks at a lower critical load. On the other hand, micropore location did not significantly impact fracture evolution.

(4) The XFEM results were in good agreement with the experimental load-displacement response for the control and 0.3 wt/wt % group, but there were variations in the stiffness in the other groups.

These experimental and numerical K_{IC} findings suggest that 1.2 and 2.4 wt/wt % of telavancin is a promising loading weight for clinical use, and that porosity must be reduced and controlled when clinicians use telavancin-loaded bone cement for arthroplasty.

Conflict of Interest

The authors declare that there is no conflict of interest associated with this study.

Funding Data

- Theravance Biopharma US, Inc., South San Francisco, CA (Grant No. TLV-2016-002; Funder ID: 10.13039/100013993).

References

[1] Lewis, G., 1997, "Properties of Acrylic Bone Cement: State of the Art Review," J. Biomed. Mater. Res., **38**(2), pp. 155–182.

[2] Tyson, Y., Rolfson, O., Kärrholm, J., Hailer, N. P., and Mohaddes, M., 2019, "Uncemented or Cemented Revision Stems? Analysis of 2,296 First-Time Hip Revision Arthroplasties Performed Due to Aseptic Loosening,

Reported to the Swedish Hip Arthroplasty Register," Acta Orthop., **90**(5), pp. 421–426.

[3] Gundtoft, P. H., Varnum, C., Pedersen, A. B., and Overgaard, S., 2016, "The Danish Hip Arthroplasty Register," Clin. Epidemiol., **8**, pp. 509–514.

[4] Havelin, L. I., Engesaeter, L. B., Espehaug, B., Furnes, O., Lie, S. A., and Vollset, S. E., 2000, "The Norwegian Arthroplasty Register: 11 Years and 73,000 Arthroplasties," Acta Orthop. Scand., **71**(4), pp. 337–353.

[5] Stelmach, P., Wedemeyer, C., Fuest, L., Kurscheid, G., Gehrke, T., Klenke, S., Jäger, M., Kauther, M. D., and Bachmann, H. S., 2016, "The BCL2 -938C>a Promoter Polymorphism is Associated With Risk for and Time to Aseptic Loosening of Total Hip Arthroplasty," PLoS One, **11**(2), p. e0149528.

[6] Topoleski, L. D. T., Ducheyne, P., and Cukler, J. M., 1990, "A Fractographic Analysis of In Vivo Poly(Methyl Methacrylate) Bone Cement Failure Mechanisms," J. Biomed. Mater. Res., **24**(2), pp. 135–154.

[7] Jasty, M., Maloney, W. J., Bragdon, C. R., O'Connor, D. O., Haire, T., and Harris, W. H., 1991, "The Initiation of Failure in Cemented Femoral Components of Hip Arthroplasties," J. Bone Jt. Surg. Br., **73-B**(4), pp. 551–558.

[8] Jaffe, W. L., Rose, R. M., and Radin, E. L., 1974, "On the Stability of the Mechanical Properties of Self-Curing Acrylic Bone Cement," J. Bone Jt. Surg. Am., **56**(8), pp. 1711–1714.

[9] Lautenschlager, E. P., Marshall, G. W., Marks, K. E., Schwartz, J., and Nelson, C. L., 1976, "Mechanical Strength of Acrylic Bone Cements Impregnated With Antibiotics," J. Biomed. Mater. Res., **10**(6), pp. 837–845.

[10] Davies, J. P., O'Connor, D. O., Burke, D. W., and Harris, W. H., 1989, "Influence of Antibiotic Impregnation on the Fatigue Life of Simplex P and Palacos R Acrylic Bone Cements, With and Without Centrifugation," J. Biomed. Mater. Res., **23**(4), pp. 379–397.

[11] Carter, D. R., Gates, E. I., and Harris, W. H., 1982, "Strain-Controlled Fatigue of Acrylic Bone Cement," J. Biomed. Mater. Res., **16**(5), pp. 647–657.

[12] Armstrong, M. S., Spencer, R. F., Cunningham, J. L., Gheduzz, S., Miles, A. W., and Learmonth, I. D., 2002, "Mechanical Characteristics of Antibiotic-Laden Bone Cement," Acta Orthop. Scand., **73**(6), pp. 688–690.

[13] Sanz-Ruiz, P., Paz, E., Abenojar, J., del Real, J. C., Vaquero, J., and Forriol, F., 2014, "Effects of Vancomycin, Cefazolin and Test Conditions on the Wear Behavior of Bone Cement," J. Arthroplasty, **29**(1), pp. 16–22.

[14] van de Belt, H., Neut, D., Uges, D. R., Schenk, W., van Horn, J. R., van der Mei, H. C., and Busscher, H. J., 2000, "Surface Roughness, Porosity and Wettability of Gentamicin-Loaded Bone Cements and Their Antibiotic Release," Biomaterials, **21**(19), pp. 1981–1987.

[15] Ishihara, S., McEvily, A. J., Goshima, T., Kanekasu, K., and Nara, T., 2000, "On Fatigue Lifetimes and Fatigue Crack Growth Behavior of Bone Cement," J. Mater. Sci. Mater. Med., **11**(10), pp. 661–666.

[16] Sinnett-Jones, P. E., Browne, M., Moffat, A. J., Jeffers, J. R., Saffari, N., Buffière, J. Y., and Sinclair, I., 2009, "Crack Initiation Processes in Acrylic Bone Cement," J. Biomed. Mater. Res. A, **89A**(4), pp. 1088–1097.

[17] Karpiński, R., Szabelski, J., and Maksymiuk, J., 2019, "Effect of Physiological Fluids Contamination on Selected Mechanical Properties of Acrylate Bone Cement," Mater., **12**(23), p. 3963.

[18] Dunne, N. J., Orr, J. F., Mushipe, M. T., and Eveleigh, R. J., 2003, "The Relationship Between Porosity and Fatigue Characteristics of Bone Cements," Biomaterials, **24**(2), pp. 239–245.

[19] Murphy, B. P., and Prendergast, P. J., 2000, "On the Magnitude and Variability of the Fatigue Strength of Acrylic Bone Cement," Int. J. Fatigue, **22**(10), pp. 855–864.

[20] Hosseinzadeh, H. R. S., Emami, M., Lahiji, F., Shahi, A. S., Masoudi, A., and Emami, S., 2013, *The Acrylic Bone Cement in Arthroplasty*, InTech, Rijeka, Croatia, pp. 101–128 (Arthroplasty—Update).

[21] Hoey, D., and Taylor, D., 2009, "Quantitative Analysis of the Effect of Porosity on the Fatigue Strength of Bone Cement," Acta Biomater., **5**(2), pp. 719–26.

[22] Jeffers, J. R. T., Browne, M., Roques, A., and Taylor, M., 2005, "On the Importance of Considering Porosity When Simulating the Fatigue of Bone Cement," ASME J. Biomech. Eng., **127**(4), pp. 563–570.

[23] Heidari-Rarani, M., and Sayedain, M., 2019, "Finite Element Modeling Strategies for 2D and 3D Delamination Propagation in Composite DCB Specimens Using VCCT, CZM and XFEM Approaches," Theor. Appl. Fract. Mech., **103**, p. 102246.

[24] Idkaidek, A., and Jasiuk, I., 2017, "Cortical Bone Fracture Analysis Using XFEM—Case Study," Int. J. Numer. Method Biomed. Eng., **33**(4).

[25] Rudraraju, S. S., Salvi, A., Garikipati, K., and Waas, A. M., 2010, "In-Plane Fracture of Laminated Fiber Reinforced Composites With Varying Fracture Resistance: Experimental Observations and Numerical Crack Propagation Simulations," Int. J. Solids Struct., **47**(7–8), pp. 901–911.

[26] Bishop, A. R., Kim, S., Squire, M. W., Rose, W. E., and Ploeg, H. L., 2018, "Vancomycin Elution, Activity and Impact on Mechanical Properties When Added to Orthopedic Bone Cement," J. Mech. Behav. Biomed. Mater., **87**, pp. 80–86.

[27] Slane, J. A., Vivanco, J. F., Rose, W. E., Squire, M. W., and Ploeg, H. L., 2014, "The Influence of Low Concentrations of a Water Soluble Poragen on the Material Properties, Antibiotic Release, and Biofilm Inhibition of an Acrylic Bone Cement," Mater. Sci. Eng. C Mater. Biol. Appl., **42**, pp. 168–176.

[28] Kim, S., Bishop, A. R., Squire, M. W., Rose, W. E., and Ploeg, H. L., 2020, "Mechanical, Elution, and Antibacterial Properties of Simplex Bone Cement Loaded With Vancomycin," J. Mech. Behav. Biomed. Mater., **103**, p. 103588.

[29] Hu, X. Y., Liu, Z. L., and Zhuang, Z., 2017, "XFEM Study of Crack Propagation in Logs After Growth Stress Relaxation and Drying Stress Accumulation," Wood Sci. Technol., **51**(6), pp. 1447–1468.

[30] Mubashar, A., Ashcroft, I. A., and Crocombe, A. D., 2014, "Modelling Damage and Failure in Adhesive Joints Using a Combined XFEM-Cohesive Element Methodology," J. Adhes., **90**(8), pp. 682–697.

[31] Orr, J. F., Dunne, N. J., and Quinn, J. C., 2003, "Shrinkage Stresses in Bone Cement," Biomaterials, **24**(17), pp. 2933–2940.

[32] Ziegler, T., and Jaeger, R., 2020, "Fracture Toughness and Crack Resistance Curves of Acrylic Bone Cements," J. Biomed. Mater. Res. Part B Appl. Biomater., **108**(5), pp. 1961–1971.

[33] Lewis, G., 1994, "Effect of Methylene Blue on the Fracture Toughness of Acrylic Bone Cement," Biomaterials, **15**(12), pp. 1024–1028.

[34] Lewis, G., and Mladsi, S., 2000, "Correlation Between Impact Strength and Fracture Toughness of PMMA-Based Bone Cements," Biomaterials, **21**(8), pp. 775–781.

[35] Lewis, G., 2009, "Properties of Antibiotic-Loaded Acrylic Bone Cements for Use in Cemented Arthroplasties: A State-of-the-Art Review," J. Biomed. Mater. Res. B Appl. Biomater., **89B**(2), pp. 558–574.

[36] Krause, W. R., and Hofmann, A., 1989, "Antibiotic Impregnated Acrylic Bone Cements: A Comparative Study of the Mechanical Properties," J. Bioactive Compatible Polym., **4**(4), pp. 345–361.

[37] Hoey, D., and Taylor, D., 2008, "Fatigue in Porous PMMA: The Effect of Stress Concentrations," Int. J. Fatigue, **30**(6), pp. 989–995.

[38] Ling, R. S., and Lee, A. J., 1998, "Porosity Reduction in Acrylic Cement is Clinically Irrelevant," Clin. Orthop. Relat. Res., (355), pp. 249–253.

[39] Gustafsson, A., Wallin, M., and Isaksson, H., 2019, "Age-Related Properties at the Microscale Affect Crack Propagation in Cortical Bone," J. Biomech., **95**, p. 109326.

[40] Gustafsson, A., Khayyeri, H., Wallin, M., and Isaksson, H., 2019, "An Interface Damage Model That Captures Crack Propagation at the Microscale in Cortical Bone Using XFEM," J. Mech. Behav. Biomed. Mater., **90**, pp. 556–565.

[41] Meyer, J., Piller, G., Spiegel, C. A., Hetzel, S., and Squire, M., 2011, "Vacuum-Mixing Significantly Changes Antibiotic Elution Characteristics of Commercially Available Antibiotic-Impregnated Bone Cements," J. Bone Jt. Surg. Am., **93**(22), pp. 2049–2056.

[42] Topoleski, L. D. T., Ducheyne, P., and Cuckler, J. M., 1993, "Microstructural Pathway of Fracture in Poly(Methyl Methacrylate) Bone Cement," Biomaterials, **14**(15), pp. 1165–1172.

[43] Jiranek, W. A., Hanssen, A. D., and Greenwald, A. S., 2006, "Antibiotic-Loaded Bone Cement for Infection Prophylaxis in Total Joint Replacement," J. Bone Jt. Surg. Am., **88**(11), pp. 2487–2500.

[44] Entezari, A., Roohani-Esfahani, S. I., Zhang, Z., Zreiqat, H., Dunstan, C. R., and Li, Q., 2016, "Fracture Behaviors of Ceramic Tissue Scaffolds for Load Bearing Applications," Sci. Rep., **6**(1), p. 28816.

[45] Pazhouheshgar, A., Vanini, S. A. S., and Moghanian, A., 2019, "The Experimental and Numerical Study of Fracture Behavior of 58 s Bioactive Glass/Polysulfone Composite Using the Extended Finite Elements Method," Mater. Res. Express, **6**(9), p. 095208.

[46] Garikipati, K., Waas, A., Bednarcyk, B., and Rudraraju, S., 2013, "On the Theory and Numerical Simulation of Cohesive Crack Propagation With Application to Fiber-Reinforced Composites," NASA, Washington, DC, Report No. NASA/TP-2013-217431.

[47] Hasenwinkel, J. M., Lautenschlager, E. P., Wixson, R. L., and Gilbert, J. L., 2002, "Effect of Initiation Chemistry on the Fracture Toughness, Fatigue Strength, and Residual Monomer Content of a Novel High-Viscosity, Two-Solution Acrylic Bone Cement," J. Biomed. Mater. Res., **59**(3), pp. 411–421.